Article ID: 1671-3664(2007)03-0215-09 **DOI**: 10.1007/s11803-007-0762-y

Near-fault ground motions with prominent acceleration pulses: pulse characteristics and ductility demand

Mai Tong[1†], Vladimir Rzhevsky[1‡], Dai Junwu[2§], George C Lee[1§], Qi Jincheng[1§] and Qi Xiaozhai[2§]

1. *MCEER, State University of New York at Buffalo, USA*
2. *Institute of Enginering Mechanics, China Earthquake Administration, Harbin 150080, China*

Abstract: Major earthquakes of last 15 years (e.g., Northridge 1994, Kobe 1995 and Chi-Chi 1999) have shown that many near-fault ground motions possess prominent acceleration pulses. Some of the prominent ground acceleration pulses are related to large ground velocity pulses, others are caused by mechanisms that are totally different from those causing the velocity pulses or fling steps. Various efforts to model acceleration pulses have been reported in the literature. In this paper, research results from a recent study of acceleration pulse prominent ground motions and an analysis of structural damage induced by acceleration pulses are summarized. The main results of the study include: (1) temporal characteristics of acceleration pulses; (2) ductility demand spectrum of simple acceleration pulses with respect to equivalent classes of dynamic systems and pulse characteristic parameters; and (3) estimation of fundamental period change under the excitation of strong acceleration pulses. By using the acceleration pulse induced linear acceleration spectrum and the ductility demand spectrum, a simple procedure has been developed to estimate the ductility demand and the fundamental period change of a reinforced concrete (RC) structure under the impact of a strong acceleration pulse.

Keywords: near-fault ground motions; acceleration pulse; ductility demand spectrum

1 Introduction

Near-fault ground motion characteristics have been extensively researched since several major earthquakes occurred in the 1990's (Hall *et al*., 1995; Sommerville *et al*., 1997; Alavi and Krawinkler, 2000; Mavroedis *et al*., 2004). The primary near-fault ground motion characteristics include: permanent static displacement and fling step caused by ground movement; impulse velocity and directivity effect caused by directional fault rupture mechanism; and large acceleration spikes caused by fault rupture dynamics. While the main research interests focused on the velocity pulses, which often produce strong low frequency fault-normal components in the ground motions, some recent studies (Tong *et al*., 2002; Markris and Black, 2004; Dai *et al*., 2004; Xie *et al*., 2005; Zhang *et al*., 2005) also indicated that prominent high frequency acceleration pulses may carry large potential damaging effects. Different from the velocity pulses, some strong acceleration pulses in a ground time history often dominate the spectral acceleration, but do not contribute significantly to spectral velocity (Dai *et al*., 2004; Zhang *et al*., 2005). Further, comparing these spectral responses to those of the ground motions without prominent acceleration pulses, it has been observed that for structures with fundamental periods falling in the resonant band of the prominent pulse, the corresponding peak responses of the structures can be significantly higher. In addition, if a sequence of consecutive acceleration pulses appears in the ground motion, the pulse effects may be compounded (Dai *et al*., 2004; Zhang *et al*., 2005).

In this paper, research results from a recent study of acceleration pulse prominent ground motions and analysis and quantification of acceleration pulse induced structural damage effects are summarized. The main results include:

(1) Temporal characteristics of acceleration pulses.

(2) Acceleration response spectra of strong acceleration pulse dominant ground motions.

(3) Estimation of structural dynamic property changes under strong acceleration pulses (e.g., increase of fundamental period for reinforced concrete (RC) structures).

2 Temporal characteristics of prominent acceleration pulses

The ground acceleration pulses in a near-fault zone (<20 km from the fault strike) can be generally

Correspondence to: Mai Tong, MCEER, State University of New York at Buffalo, Red Jacket Quadrangle, Buffalo, NY 14261-0025, USA
Tel: 716-645-3498; Fax: 716-645-3399
E-mail: mtong@mceermail.buffalo.edu
†Senior Research Scientist; ‡Emeritus Professor; §Professor

Sponsored by: U.S. National Science Foundation Under Grant CMS-0202846
Received July 21, 2007; **Accepted** July 30, 2007

classified into three types: (1) unrelated to the velocity pulses or permanent ground displacement at the site, but contributing a major portion of spectral acceleration response at the short fundamental periods; (2) directly related to velocity pulses (rupture directivity effect) or other peak values such as PGV and PGD; and (3) contributed a large fling step or displacement pulse (long period low amplitude pulses), but not obviously recognizable from ground acceleration time histories. In Figs. 1-3, a comparison of three selected ground motion records (TCU045, TCU095 and TCU051) from the Chi-Chi earthquake illustrates the characteristics of the three types of acceleration pulses. Figure 1(a) shows the prominent acceleration pulses in the TCU045 NS record. The acceleration pulses contributed more than 90% of the spectral acceleration responses (Fig. 1(b)). However, the extracted acceleration pulses do not produce the velocity pulse and displacement offset seen from the original record (Fig. 1(c)). It shows that the acceleration pulses are unrelated to the velocity pulse and permanent displacement. Note that in the record, the PGV is still controlled by the acceleration pulse; however, the main velocity pulse has a much longer duration as shown in Fig. 1(c).

Figure 2(a) shows the prominent acceleration pulses in the TCU095 NS record. The acceleration pulse is coherent to the PGV and dominates the spectral acceleration and velocity (Fig. 2(b)). Figures 2(b) and 2(c) show that the acceleration pulses alone have influenced a significant portion of the PGV and about one third of PGD.

Figure 3(a) shows the acceleration, velocity and displacement of the TCU051 NS record. It is seen that the large displacement pulse is produced from a low frequency acceleration pulse, which is hidden under the high frequency contents of the ground accelerations (Fig. 3(b)). Figure 3(c) shows the low frequency acceleration pulse produced displacement compared to the original ground displacement record.

Single or multiple acceleration pulse excitations, compared to random excitations, are relatively easy to model. Efforts to describe different waveforms of ground acceleration and velocity pulses are seen in recent publications (Mavroeidis *et al*., 2004; Makris and Black, 2004; Xie *et al*., 2005; Zhang *et al*., 2005). The most commonly used waveforms include symmetric triangle, rectangle, and half-sinusoidal of the same amplitudes and duration. A set of formulations of the simple pulses and their acceleration velocity and displacement relationship are provided (Xie *et al*., 2005). These simple pulse waveforms are applied to approximate the forward directivity and fling step effects (Mavroeidis *et al*., 2004). Figures 4(a)-(c) show the basic triangle pulse and the corresponding sequence of pulse combinations that correspond to forward directivity velocity pulse and fling step displacement pulse.

The basic characteristic parameters of the triangle pulse are the amplitude A, the half cycle duration τ and the number of pulses in the sequence. Since ground motion records are commonly given in NS, EW and UD projections, this representation is sufficient to capture the velocity pulse related aspects seen in one dimensional ground motion records. However, forward directivity typically generates stronger motion in the fault-normal direction and weaker motion in the fault-parallel direction (Dray and Rodriguez-Marek, 2004). The fault-normal and parallel directions, in most cases, do not coincide with the NS, EW and UD directions at the ground motion recording stations. Therefore, a more informative view of the ground pulse characteristics requires a two or three dimensional wave representation. Furthermore, acceleration pulses are not limited to those directly associated with the velocity pulses or fling step, as some 3 dimensional (3D) ground motion characteristics can be very different from their 1D projection (Tong *et al*., 2002).

Tong and Lee (1999) and Tong *et al*. (2002) considered a moving coordinate decomposition of 3D motion trajectory for analysis of temporal characteristics of acceleration pulses. The ground acceleration vector is recast with respect to a moving coordinate system $\{\boldsymbol{T}, \boldsymbol{N}, \boldsymbol{B}\}$, in which $\boldsymbol{T}$ and $\boldsymbol{N}$ are the tangential and normal directions of the motion at the moment in reference to the current point on the displacement trajectory. The 3D acceleration vector is then expressed as a two dimensional vector projection

$$a = a_{\mathrm{T}}\boldsymbol{T} + a_{\mathrm{N}}\boldsymbol{N} \tag{1}$$

$a_{\mathrm{N}} = \kappa|v|^2$ (v – speed of the velocity vector) represents the normal acceleration, which only changes the direction of the acceleration vector, but is independent of the speed change. $a_{\mathrm{T}} = \mathrm{d}|v|/\mathrm{d}t$ represents the tangential acceleration, which only changes the speed. Since the tangential acceleration can increase or decrease the speed, the tangential acceleration effect is separated as acceleration and deceleration, denoted as a_{T}^{+} and a_{T}^{-}, respectively. This mathematical representation simplifies the kinematic relationship between the 3D acceleration and velocity vectors.

By examining the 3D norm of ground acceleration and velocity using the 3D moving coordinate decomposition, the following relationship is derived: the velocity pulse kinetically coherent with two acceleration pulses such that the rising phase of the velocity pulse corresponds to a positive tangential acceleration (a_{T}^{+}) pulse, which increases the speed; the decaying phase of the velocity pulse corresponds to a negative tangential acceleration (a_{T}^{-}) pulse, which decreases the speed. Figure 5 illustrates this relationship through a decomposition of the PGV pulse and its corresponding normal and tangential acceleration components from the CHY028 record of the Chi-Chi earthquake.

The temporal analysis of the waveforms of the acceleration pulses can provide some useful details. For example, from Fig. 5, it is seen that the rising and decaying phases of the velocity pulse are 0.4 and 0.18 s, respectively, which correspond to the different

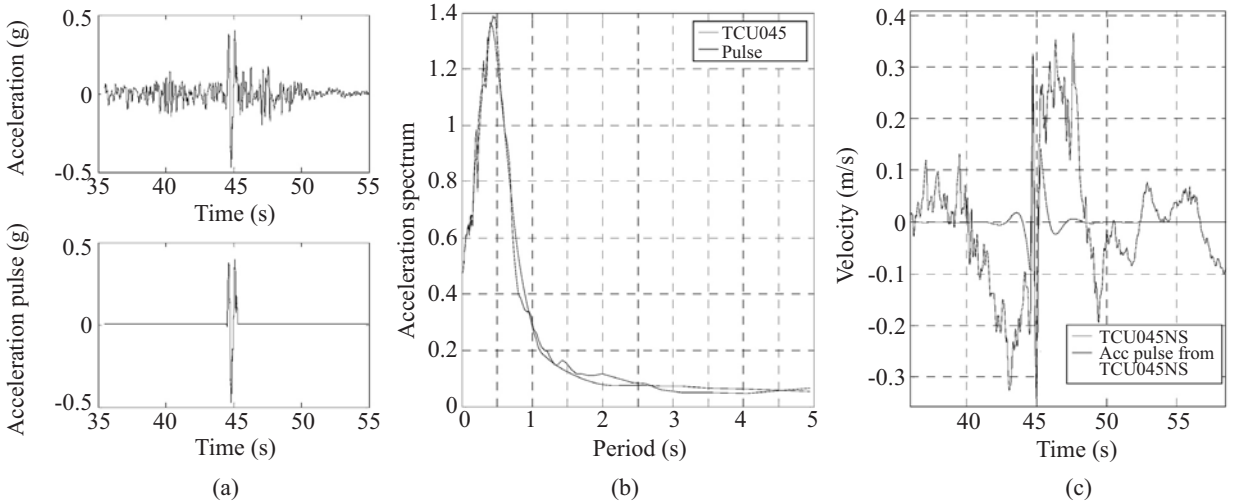

Fig. 1 TCU045 NS ground motion with prominent acceleration pulse

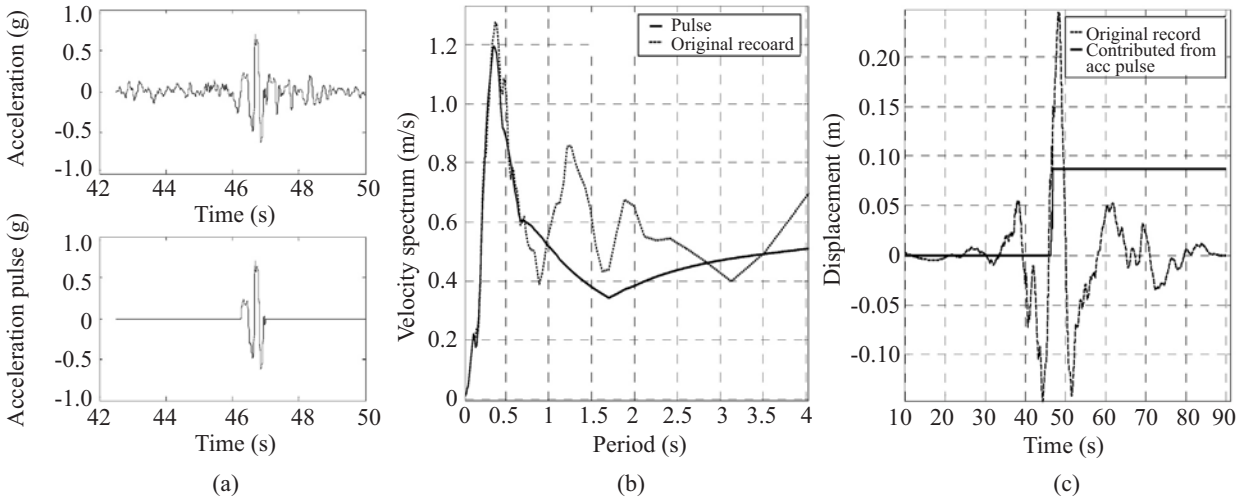

Fig. 2 TCU095 NS ground motion with prominent acceleration pulse

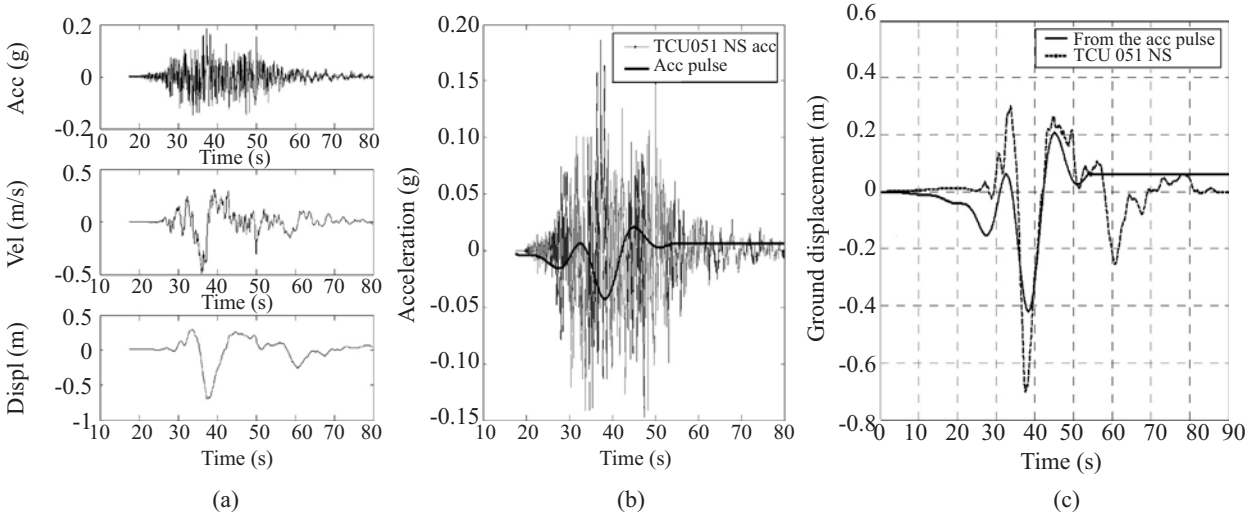

Fig. 3 TCU051 ground motion and the low frequency acceleration pulse

durations of the acceleration and deceleration pulses. The peaks of the two tangential acceleration pulses are 400 and 600 Gal, and again, the amplitudes of the two tangential acceleration pulses are significantly different. Furthermore, as shown in Fig. 5, the 3D PGV and PGA in many of the prominent acceleration pulse ground motions are coherent. However, unlike what is normally expected (i.e., where large acceleration produces large velocity) for the correlated PGA and PGV, often PGV occurs ahead of PGA. Further, a close examination of the temporal characteristics of the acceleration pulse reveals that the PGA is dominated by a large deceleration pulse.

Another temporal characteristic quantity of ground acceleration is the derivative of acceleration, which carries more details of high frequency components. Although most structures are less sensitive to the high frequency components in ground motions, the high frequency components of the derivative of accelerations are potentially good indicators of the changes in structural strength due to heavy dynamic loadings (Tong *et al*., 2005).

3 Prominent acceleration pulse induced response spectra

The structural responses excited by the ground motions with prominent acceleration pulses are generally correlated to the pulses of the excitation and dominated by only a few cycles of large pulse-like motions with coherent peak values of acceleration, velocity and displacement. Such coherent peak response values imply that there are parametric relationships between the key parameters (i.e., amplitude, duration and waveform) of the acceleration pulse and the corresponding response peak values. Therefore, pulse excited response spectra should be able to provide more useful information than traditional random excitation induced response spectra.

Consider the linear response of a SDOF system subject to an acceleration pulse excitation,

$$m\ddot{X} + c\dot{X} + k_0 X = -mG_{\mathrm{p}} \tag{2}$$

where m is mass, c is the damping coefficient, G_{p} is the full cycle ground acceleration pulse (as shown in Fig. 4(b)) with amplitude A and duration τ. X, $\dot{X}$ and $\ddot{X}$ are the displacement, velocity and acceleration responses of the system. To compare the spectral acceleration, velocity and displacement of the elastic systems, the dynamic system and the input pulse amplitude (with m=1 and A =1) is normalized. Figure 6 shows the elastic spectral acceleration. This spectrum is calculated with the amplitude of the input acceleration set to 1g. Therefore, the spectrum value can also be interpreted as the acceleration amplification factor if the input acceleration amplitude is changed to a non-unit level A. In that case, the corresponding spectral acceleration is equal to A multiplied by the corresponding amplification value from the normalized spectrum. Note that the horizontal axis of the spectrum is given in $2\tau/T_0$. This is because the pulse excited spectral acceleration of an SDOF system is invariant with respect to the period ratio $2\tau/T_0$. Namely, a system with a fundamental period of T_0 excited by a pulse of duration τ will have the same peak acceleration as a system with a fundamental period T_0 excited by a pulse of duration 2τ.

For elastic-plastic response of a SDOF system, the above dynamic equation is modified by

$$m\ddot{X} + c\dot{X} + R(X,\dot{X}) = -mG_{\mathrm{p}} \tag{3}$$

where $R(X, \dot{X})$ is the restoring force and can usually be modeled by an inelastic hysteresis function such as the trilinear function given below.

$$R(X,\dot{X}) = \begin{cases} k_e(X - x_0) & |X - x_0| \le x_1 \\ \mathrm{sign}(X - x_1)R_y + k_p(X - x_1) & x_1 < X < x_2,\ X\cdot\dot{X} > 0 \\ \mathrm{sign}(X - x_2)R_u & x_2 < X < x_3,\ X\cdot\dot{X} > 0 \\ k_r(X - x_4) & x_4 < X < x_3,\ X\cdot\dot{X} < 0 \end{cases} \tag{4}$$

For this trilinear hysteresis function, the corresponding yielding point x_1, fully yield point x_2, offload point x_3 and offset point x_4 are shown in Fig.7. Note that the definition of R is not limited to X>0 and R>0 (the first quadrant). In other quadrants, the definition is symmetric to that of the first quadrant as given in the figure.

The typical response loop shown in Fig.7 can be approximated by the trilinear model with k_{e} to be the elastic stiffness before the loop, R_{y} to be the yielding point, k_{p} to be the stiffness after the yielding point before entering plasticity, R_{u} to be the ultimate strength.

Based on the trilinear model, the total incremental displacement for a given hysteresis loop is defined to be

$$\Delta D = X_{\max} - x_0 \tag{5}$$

and the maximum elastic displacement is defined to be

$$\Delta d_{\mathrm{E}} = x_1 - x_0 \tag{6}$$

where x_0 is the initial position, x_1 is the yielding displacement, $X_{\max}$ is the maximum displacement reached in the loop. Then, the corresponding ductility of the loop is measured by

$$\mu = \begin{cases} 0 & \text{if } \Delta D \le \Delta d_{\mathrm{E}} \\ \dfrac{\Delta D - \Delta d_{\mathrm{E}}}{\Delta d_{\mathrm{E}}} & \text{if } \Delta D > \Delta d_{\mathrm{E}} \end{cases} \tag{7}$$

Consider a special case of the trilinear system with $R_{\mathrm{y}} = R_{\mathrm{u}}$. This is an elastic-perfect plastic system which reduces the trilinear model to a bilinear model.

To evaluate inelastic spectral responses induced by prominent acceleration pulses, four parameters, A, τ, T_0,

and R_y, can influence the spectral responses. To simplify the cumbersome multi-variable function, it is desirable to group the spectral response values into same-value classes such that they can be distinguished by equivalent relationships formulated with the four variables. Makris and Black (2004) looked into developing dimensionless spectral displacement of elastic and inelastic systems. In this paper, we consider dimensionless classes, $2\tau/T_0$ and R_y/R_{max}, as the basic variables of the ductility demand function, where τ is the half cycle duration of the pulse and T_0 is the fundamental period of the dynamic system; and R_y is the yielding force and R_{max} is the maximum restoring force that corresponds to the maximum elastic displacement of the dynamic system under the pulse loading. Figure 8 shows the ductility time histories of three different elastic-perfect plastic systems such

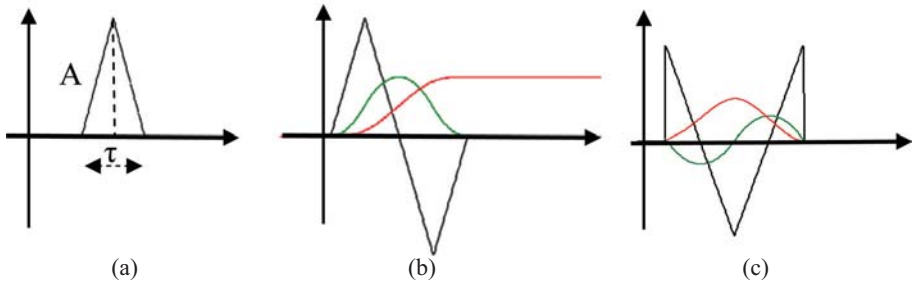

Fig. 4 Simple acceleration pulses of triangle waveform (black) with corresponding velocity (green) and displacement (red)

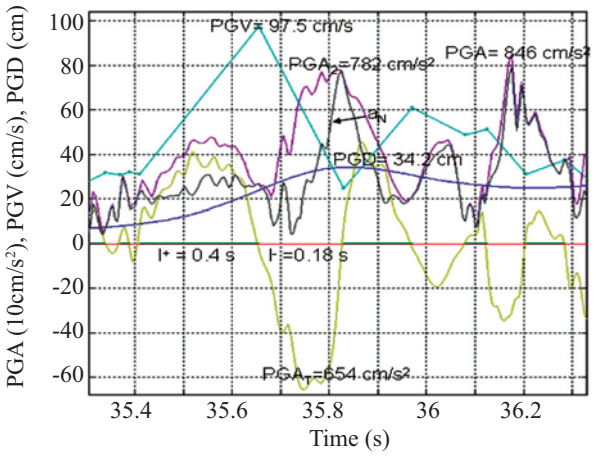

Fig. 5 Temporal characteristics analysis of Chi-Chi record CHY028

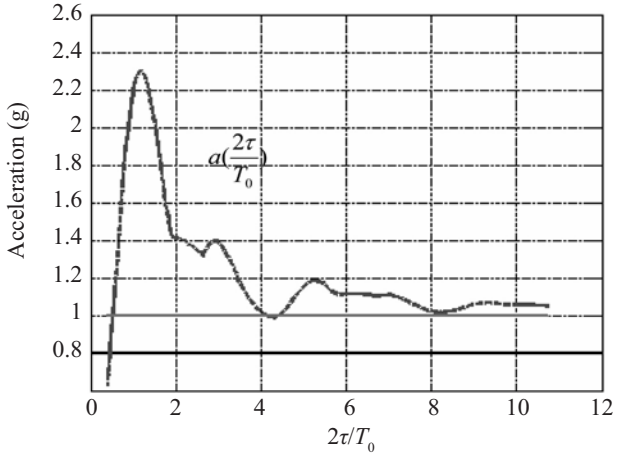

Fig. 6 Elastic acceleration spectrum under the normalized triangle pulse loading (Amplitude of input acceleration pulse = 1 g)

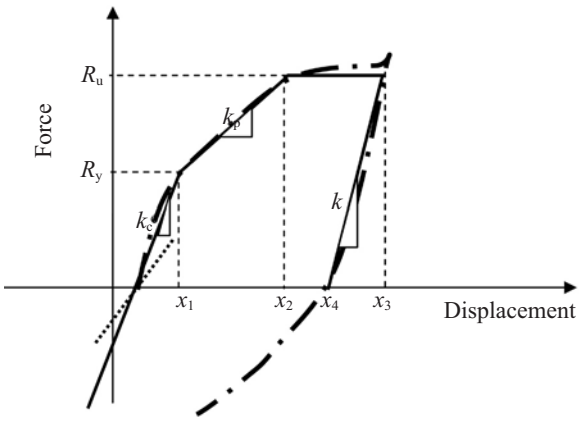

Fig. 7 A typical response loop (dotted dash line) of a normalized RC structure (m=1)

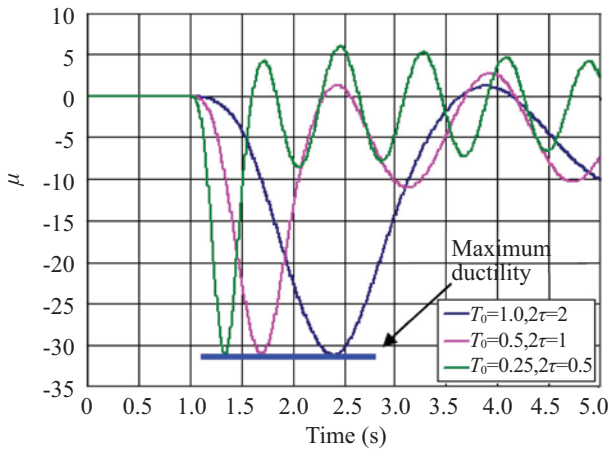

Fig. 8 Ductility time history of three different systems with T_0= 0.25; 0.5; 1.0 s excited by acceleration pulse with amplitude A= 1.0 g, and pulse durations 2τ = 0.5; 1.0 and 2.0 s

that they have different fundamental periods and are subjected to different pulse loadings; however, since $2\tau/T_0$ and R_y/R_{max} are the same, they all belong to the same class. Checking the ductility time histories, Fig. 8 shows that the peak values of ductility for all three systems are nearly identical (31.00; 30.96 and 31.14). Therefore, the equivalent class determined in this way satisfies the grouping requirements. It is shown that a ductility demand spectrum can be formulated with respect to the equivalent classes defined by $2\tau/T_0$ and R_y/R_{max}.

Figure 9 shows the ductility demand spectrum[3] as a function of $2\tau/T_0$ and R_y/R_{max}. The corresponding μ values for the equivalent classes of $2\tau/T_0$ and R_y/R_{max} are given in Table 1.

Curve-fitting the ductility demand spectral values for the equivalent classes resulted in the following empirical ductility demand spectrum with respect to the equivalent classes:

$$\mu = \sum_{i=0}^{l}\sum_{j=0}^{n} p_{ij}\left(\frac{2\tau}{T_0}\right)^i\left(\frac{R_y}{R_{max}}\right)^j \tag{8}$$

where l and n are numbers of the $2\tau/T_0$ and R_y/R_{max}, which are taken as 7 and 8, respectively. The corresponding coefficients p_{ij} are given in Table 2.

In the above ductility demand spectrum, the yielding ratio $r = R_y/R_{max}$ is an intermediate variable. It depends on the seismic-force-resisting system of the structure and the excitation pulse characteristic parameters (A and τ). The yielding ratio r is determined based on the maximum elastic displacement and the elastic response of the structure under the specified pulse loading. The maximum elastic displacement δe of a type of structure can be assessed as shown in the second column of Table 3 (derived based on Recommended Provision of SNiP, 1986). The corresponding yielding ratio r is then calculated by

$$r = \frac{R_y}{R_{max}} = \left(\frac{k_0}{m}\right)\frac{\delta_e}{a\left(\frac{2\tau}{T_0}\right)A} = \frac{4\pi\delta_e}{T_o^2 a\left(\frac{2\tau}{T_0}\right)A} \tag{9}$$

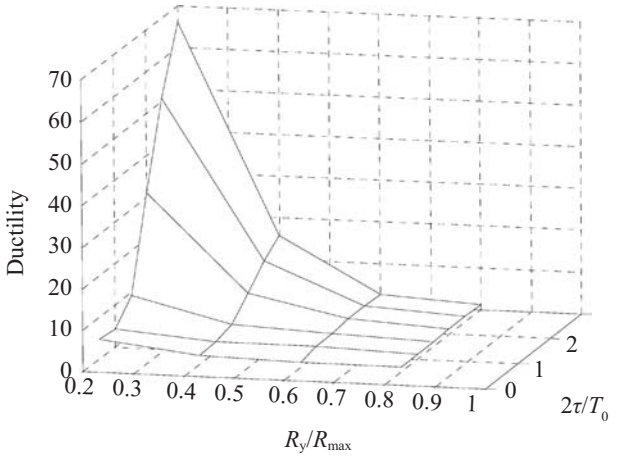

Fig. 9 Ductility demand spectrum with respect to the equivalent $2\tau/T_0$ and R_y/R_{max} classes

Table 1 Ductility demand spectrum with respect to equivalent $2\tau/T_0$ and R_y/R_{max} classes

$2\tau/T_o$	R_y/R_{max}							
	0.1	0.2	0.3	0.4	0.5	0.6	0.7	0.8
0.50	10.80	4.72	2.81	1.94	1.48	1.38	1.33	1.29
0.75	11.20	4.28	2.34	1.97	1.88	1.91	1.53	1.29
1.00	13.50	4.38	2.46	2.29	2.07	1.95	1.59	1.29
1.50	30.90	9.46	4.10	2.76	2.07	1.70	1.65	1.32
2.00	91.50	31.10	13.92	7.10	3.92	2.46	1.72	1.38
2.50	151.10	50.60	22.31	10.50	5.39	3.03	1.88	1.38
3.00	207.00	66.00	27.32	12.27	5.59	2.66	1.55	1.25

Table 2 Coefficients p_{ij} for the ductility demand spectrum

i	j							
	1	2	3	4	5	**6**	**7**	**8**
1	9532.88	-21743.45	13679.58	4211.97	-9066.98	4388.51	-953.9	89.75
2	-84460.32	185180.3	-98142.22	-65847.16	98259.3	-44861.6	9464.81	-870.32
3	295383.6	-626072	274350	317849.6	-399527.5	175459.6	-36122.43	3246.52
4	-515416.7	1065309	-385005.6	-680775.6	780371.8	-333790.7	67258.15	-5900.21
5	433285.1	-836482.8	126787.7	831523.7	-826212.4	338451.7	-66175.77	5626.81
6	-140966.3	198617.6	194740.8	-572315.2	463349.4	-176147	32854.37	-2680.17
7	11193.31	10219.58	-98132.54	150438.8	-104262.9	36965.68	-6609.33	523.19

where m is the total mass of the structure, a($2\tau/T_0$) is the elastic acceleration amplification factor (Fig. 6), T_0 is the fundamental period of the structure, and A is the amplitude of the excitation pulse.

4 Change of fundamental period under acceleration pulse excitation

Using the ductility demand spectrum developed above, the ductility demand to a structure subjected to the impact of a given acceleration pulse excitation is estimated. With this information, the potential damage to an RC structure can be evaluated in terms of its change in stiffness, fundamental period, and total plastic energy accumulation.

The corresponding stiffness degradation for RC structures is fitted by the following function (Rzhevsky and Lee, 1999)

$$\sigma = \frac{1}{(\mu + \sqrt{\mu^2 + 1})^{\gamma}} \tag{10}$$

where γ is the stiffness degradation coefficient. Note that if μ is zero, σ =1 (i.e., without plastic deformation); otherwise, if $\mu > 0$, then $\sigma < 1$, which implies that the stiffness is softened due to yielding and plastic deformation.

The degraded effective stiffness after one hysteresis loop is estimated as

$$k_0^1 = \sigma k_0 \tag{11}$$

Thus, the change of fundamental period is

$$\Delta T = T_0^1 - T_0 = 2\pi\sqrt{\frac{m}{k_0}}\left(\frac{1-\sqrt{\sigma}}{\sqrt{\sigma}}\right) = T_0\left(\frac{1-\sqrt{\sigma}}{\sqrt{\sigma}}\right) \tag{12}$$

where m is the mass of the dynamic system. The corresponding plastic energy accumulation from the plastic deformation is calculated by

$$W = \int_{\text{loop}} R(X, \dot{X})\mathrm{d}x \tag{13}$$

Based on the above formulations, a simple procedure has been developed to estimate the ductility demand and the fundamental period change for RC structures when subjected to the excitation of a prominent acceleration pulse. The basic information needed to complete the procedure include: the characteristic parameters of the acceleration pulse (amplitude A, duration τ), the initial fundamental period of the structure T_0, and the type of structure (e.g., RC moment frame). The procedure is as follows:

(1) Use the parameters of the acceleration pulse (amplitude A, duration τ) and the initial fundamental period of the structure T_0 to determine the peak acceleration level of the corresponding elastic system $a_{\max} = A\times$ (amplification factor).

(2) Use $a_{\max}$ and the structure type to determine the yielding ratio $r = R_y/R_{\max}$ where $R_{\max} = ma_{\max}$ and $R_y = r\%\ R_{\max}$. Note that knowing the general strength of the structure is often sufficient to determine the ratio r without information about the total mass (m) of the structure.

(3) Use $2\tau/T_0$ and $R_y/R_{\max}$ from steps 1 and 2 to obtain the ductility demand μ.

(4) Apply the ductility demand μ from step 3 in the stiffness degradation formula to determine the change of stiffness degradation σ and $k^1_{0.}$

(5) Use the stiffness degradation coefficient σ to determine the change of fundamental period ΔT.

The following example illustrates the use of the procedure.

Consider a structural system with T_0 = 0.5 sec. excited by a pulse of intensity A = 0.5 g, and duration τ = 0.165 s, which resembles a pulse in the Chi-Chi TCU068-90P record. $2\tau/T_0$ = 0.66. The corresponding linear acceleration amplification factor for $2\tau/T_0$ = 0.66 is 2.0 (Fig. 6). The maximum linear system spectral acceleration is $a_{\max}$ = 0.5 × 2.0= 1.0g. The ordinary RC structure under consideration has the limit elastic deflection of 0.004 (Table 3). The corresponding yielding

Table 3 Limit of elastic deflection of different structures

Seismic-force-resisting system	Maximum elastic deflection δ_e (rad)
1 story RC frame structure with 0.75% reinforcement	0.003
1 story RC frame structure with 1.5% reinforcement	0.006
1 story RC frame structure with 2.75% reinforcement	0.009
RC moment resistant frame with 0.75% reinforcement	0.002
RC moment resistant frame with 1.75% reinforcement	0.004
Masonry walls	0.003
Steel moment resistant frames	0.010

ratio $r = R_y / R_{\max} = 4 \times 3.14 \times 0.004 / 0.5^2 \times 2 \times 0.5 \approx 20\%$. For $R_y/R_{\max}$ = 20%., and $2\tau/T_0$ = 0.66, from the ductility demand spectrum of the equivalent classes, μ = 4.2. The coefficient of stiffness degradation is $\sigma = 1/((4.2 + \sqrt{4.2^2 + 1})^{\gamma} = 0.34$ (for γ = 0.5). It follows that the change of fundamental period is $\Delta T = 0.5(1 - \sqrt{.34}) / \sqrt{.34} = 0.35$ s.

An experimental verification of the above proposed methodology was carried out on simple one-story RC column-diaphragm models. The details of the experimental study are reported Part II of this paper. Table 4 summarizes the comparison between the calculated and measured change of fundamental period under various pulse inputs. Where R_y is the yielding point, $R_{\max}$ and $D_{\max}$ are maximum restoring force and displacement, respectively.

The structure stiffness of the RC models before and after each pulse loading, given in columns 2–3, are obtained from the hysterisis loop of the response acceleration versus displacement. The corresponding fundamental periods, given in columns 4-5, are obtained from the free decaying vibration of the acceleration time histories. The changes of the fundamental period calculated from the above procedure are shown in Table 5 and compared with the measured change of period ΔT.

Table 4 Results of Structural fundamental period change of the RC models

Model and event	Stiffness k_0, (10kN/m)		Fundamental period, T (s)		ΔT(s)	R_y (10kN)	$R_{\max,}$ (10kN)	$D_{\max,}$ (cm)
	Start	Finish	Start	Finish				
M #1, v104 CHY080	280	95	0.307	0.526	0.219	1.30	2.70	2.50
M#2,Ev203 CHY080	260	63	0.319	0.65	0.331	1.30	2.83	4.00
M#3, Ev304 CHY080P	220	60	0.347	0.67	0.323	1.35	2.65	3.90

Table 5 Calculated ΔT compared with measured ΔT

Model and event	X_1 (cm)	μ	σ	$\Delta T_{\text{calculated}}$(s)	Measured/Calculated
Model #1, v104 CHY080	0.464	4.38	0.34	0.225	0.97
Model #2,Ev203 CHY080	0.500	7.00	0.27	0.300	1.10
Model #3, Ev304 HY080P	0.614	5.36	0.30	0.285	1.13

5 Concluding remarks

Large acceleration spikes caused by fault rupture dynamics constitute one of the primary near-fault ground motion characteristics. In this paper, research results from a recent study of acceleration pulse prominent ground motions and an analysis of structural damage induced by acceleration pulses are summarized. The main results of the study include: (1) temporal characteristics of acceleration pulses; (2) ductility demand spectrum of simple acceleration pulses with respect to equivalent classes of dynamic systems and pulse characteristic parameters; and (3) estimation of reinforced concrete (RC) structural dynamic property changes under strong acceleration pulses.

For a reinforced concrete (RC) structural system, a simple procedure has been developed to estimate the ductility demand and the fundamental period change of the structure under the impact of a given strong acceleration pulse. The procedure consists of three calculation steps; first to obtain a ratio of the structure's yielding strength over the elastic load demand from the acceleration pulse and a ratio of pulse duration over the effective period; second to input the two ratios into the ductility demand spectrum to acquire the needed ductility demand; and finally to determine the in-cycle degradation of strength and change of fundamental period.

Acknowledgement

The research reported in this paper was sponsored by the National Science Foundation. Authors appreciate the support by NSF grant CMS-0202846.

References

Alavi B and Krawinkler H (2000), "Consideration of Near-fault Ground Motion Effects in Seismic Design,"

Proc. 12th World Conf. on Earthquake Engineering, Auckland, New Zealand, 2004.

Dai JW, Tong M, Lee GC, Qi X and Bai W (2004), "Dynamic Responses Under the Excitation of Pulse Sequences," *Earthquake Engineering and Engineering Vibration*, **3**(2):157-169.

Dray J and Rodriguez-Marek A (2004), "Characterization of Forward-directivity Ground Motions in the Near-fault Region," *Soil Dynamics and Earthquake Engineering*, (24): 815-828.

Hall John F, Heaton TH, Halling MW and Wald DJ (1995), "Near-source Ground Motion and Its Effects on Flexible Buildings," *Earthquake Spectra*, **11**(4): 569-605.

Lee GC, Tong M and Tao R (2000), "Temporal Characteristics of Chi-Chi Earthquake Ground Motion and Their Possible Implications on Structural Damages," *International Workshop on Annual Commemoration of Chi-Chi Earthquake*, Taipei.

Makris N and Black C (2004), "Dimensional Analysis of Rigid-plastic and Elastoplastic Structures Under Pulse-type Excitations," *Journal of Engineering Mechanics*, ASCE, **130**(9): 1006-1018.

Mavroeidis GP, Dong G and Papageorgiou AS (2004), "Near-fault Ground Motions and the Response of Elastic and Inelastic Single-degree-of-freedom (SDOF) Systems," *Earthquake Engineering and Structural Dynamics*, **33**: 1023-1049.

Rzhevsky VA (1990), "Seismic Resistance of Structures Subjected to Strong Earthquake Motions," *Science*, Tashkent, USSR, pp.258. (in Russian).

Rzhevsky VA and Lee GC (1999), "Seismic Response Analysis of Inelastic Non-stationary Structural Systems," *15th International Conference on Structural Mechanics in Reaction Technology (SMiRT-15)*, Seoul, Korea, August 15-20, (ID: K4-A1-US).

Rzhevsky VA, Tsipenuk IF and Khakimov SA (1996), *Code of the Republic of Uzbekistan for Seismic Regulations for Buildings and Other Structures, KMK 2.01.03-96*, Construction Committee of the Republic of Uzbekistan, Tashkent, Uzbekistan, pp.65. (in Russian)

Recommended Provision of SNiP2.03-84 Part II Chapter B (1986) *Construction Code and Regulations, Concrete and Reinforced Concrete Structures*, Moscow, Gosstroy.

Somerville PG, Smith NF, Graves RW and Abrahamson NA (1997), "Modification of Empirical Strong Ground Motion Attenuation Relations to Include the Amplitude and Duration Effects of Rupture Directivity," *Seismological Research Letter*, **68**: 199-222.

Tong M and Lee GC (1999), "3D Temporal Characteristics of Earthquake Ground Motion at a Single Point", *Journal of Engineering Mechanics*, ASCE, **125**(10): 1099-1105.

Tong M, Lee GC and Xu Y (2006), "Seismic Responses of Highway Bridges Under Near-fault Acceleration Pulses Excitation," *Forth International Workshop on Seismic Design and Retrofit of Transportation Facilities*, San Francisco, March 2006.

Tong M, Qi JC and Lee GC (2002), "Temporal a_N and a_T in Earthquake Ground Motion Analysis," *Journal of Engineering Mechanics*, ASCE, **128**(5): 502-510.

Tong M, Wang GQ and Lee GC (2005), "Time Derivative of Earthquake Acceleration," *Earthquake Engineering and Engineering Vibration*, **4**(1): pp1-16

Xie LL, Xu LJ and Rodriguez-Marek A (2005), "Representation of Near-fault Pulse-type Ground Motion," *Earthquake Engineering and Engineering Vibration*, **4**(2): 191-199.

Zhang YS, Hu YX, Zhao FX, Liang JW and Yang CH (2005), "Identification of Acceleration Pulses in Near-Fault Ground Motion Using EMD Method," *Earthquake Engineering and Engineering Vibration*, **4**(2): 201-212.